

UNIVERSITY of CALIFORNIA
SANTA CRUZ

**THERMAL EVOLUTION OF URANUS AND NEPTUNE WITH
CONDENSATION-INHIBITED CONVECTION**

A thesis submitted in partial satisfaction of the
requirements for the degree of

BACHELOR OF SCIENCE

in

ASTROPHYSICS

by

Robert Schroder

December 2020

Contents

List of Figures	v
1 Introduction	1
1.1 Condensation in Hydrogen Dominated Atmospheres	4
2 Model	6
2.1 Three-layer Model with Dry Adiabat	6
2.2 Inclusion of Moist Adiabat Within Outer Envelope	9
2.3 Temperature Jump Across the Water Condensation Zone	13
2.4 Energy Conservation and Thermal Evolution of Model	14
3 Results	16
3.1 Condensation-inhibited Convection	16
3.2 Formation of Radiative Zone	17
3.3 Thermal Evolution of Uranus and Neptune	19
4 Discussion and Conclusions	27

List of Figures

2.1	A Standard Interior Structure Model	8
2.2	Interior Structure for Moist Adiabat	11
2.3	A Standard Interior Structure Model	12
3.1	Inhibition of convection on Uranus	18
3.2	Impact of Radiative Layer on T10	20
3.3	Formation of Radiative Zone	22
3.4	Thermal Evolution Curves for Uranus - Adiabat Comparisons	23
3.5	Thermal Evolution Curves for Uranus - Water Vapor Concentration Comparisons	24
3.6	Thermal Evolution Curves for Neptune - Water Vapor Concentration Comparisons	25
3.7	Thermal Evolution Curves for Uranus - Radius	26
3.8	Thermal Evolution Curves for Neptune - Radius	26

1

Introduction

Planets coalesce from matter contained in their parent star's protoplanetary disk.

A planet will accrete matter from the disk until the supply is exhausted, at which point, the planet will begin to cool and contract over time (cite armitage and lissauer). When discussing cooling, it will be necessary to define what we mean when talking about the temperature of a planet, as there are several temperatures that describe a planet's temperature. The effective temperature, T_{eff} , is defined as the total flux integrated over all frequencies, ν , of a black body of the same shape and same distance as the planet (Seager, 2010):

$$\pi \int_0^{\infty} B(T, \nu) d\nu = \sigma_B T_{\text{eff}}^4 \quad (1.1)$$

Here, σ_B is the Stefan-Boltzmann constant, and F_{\star} is the stellar flux. Simplifying further, this yields

$$T_{\text{eff}} = \left(\frac{F_{\star}}{\sigma_B} \right)^{\frac{1}{4}}. \quad (1.2)$$

The equilibrium temperature, T_{eq} , is the temperature the planet would have if it were in thermal equilibrium with its parent star. This occurs when the planet has radiated away

its latent heat of formation, and the only remaining source of energy is from its star. This temperature is defined as

$$T_{\text{eq}}^4 = \frac{F_\star(1 - A_B)}{r_{\text{au}}^2 4\pi\sigma_B} * * * \text{REEXAMINE} \quad (1.3)$$

where r_{au} is the distance from the star in AU, A_B is the bond albedo. Finally, the intrinsic temperature, T_{int} , the temperature that defines the flux from the planet's interior and is defined by the relation

$$T_{\text{eff}}^4 = T_{\text{eq}}^4 + T_{\text{int}}^4. \quad (1.4)$$

In 1965, Frank Low measured Jupiter's intrinsic temperature (Low, 1966). To explain this observation, theorists set out to expand on prior work by (Demarcus, 1958) on the theory of interior structure of solar system gas and ice giants (Hubbard, 1968; Smoluchowski, 1967; Hubbard, 1977, 1978; M. Podolak, 1991). These models assumed that the interior of giant planets are convective, meaning that heat within the planet's interior is transferred by the movement of fluids. In other words, warmer, less dense material will rise; while cooler, more dense material will sink due to the influence of gravity. In 1968, Hubbard showed that a convective interior would allow Jupiter's observed flux to be transported to the surface adiabatically. This analysis motivated the inclusion of adiabatic interiors in contemporary interior structure models for gas and ice giants.

At the present time, most of the giant planets in our solar system: Saturn, Jupiter, and Neptune, all have an intrinsic flux. Uranus is the exception (Pearl & Conrath, 1991). Measurements of Uranus's effective temperature are consistent with a planet that has no intrinsic flux, a planet in thermal equilibrium with the Sun, cooler than its more distant neighbor, Neptune, a planet of similar mass and composition.

While thermal evolution models do currently reproduce T_{eff} for Jupiter and Neptune at 4.6 Gyr (Graboske et al., 1975; Fortney et al., 2011), they do not reproduce T_{eff} for Saturn and Uranus. Models for Saturn predict a cooler planet; however, plausible explanations have been offered to explain its current, warmer T_{eff} . Among them, the rain-out of helium (Fortney & Hubbard, 2003; Mankovich & Fortney, 2019), or double-diffusive convection (Leconte & Chabrier, 2013).

Meanwhile, for Uranus, the models have predicted a warmer effective temperature at present time (Fortney et al., 2011; M. Podolak, 1991; W.B. Hubbard, 1995; L. Scheibe, 2019). There have been various attempts to explain Uranus' cool temperature. Early investigations posited that a stratified interior, stable against convection, would allow heat to be trapped deep within the the interior (M. Podolak, 1991). If in fact, the interior of a planet were stable against against convection, some other means of energy transport must be responsible for transporting heat from the interior to the surface. Possible mechanisms include conduction, radiative diffusion, or perhaps double-diffusive convection. Later work investigated some of the other possible mechanisms for energy transport. (Guillot, 1995) posited that condensates such as NH_3 , CH_4 , or H_2O when at critical abundance could interfere with convection, producing temperature profiles that would be superadiabatic. (Nettelmann et al., 2016) looked at the inclusion of ad-hoc thermal boundary layers within a planet's interior and found that they could possibly explain Uranus's current T_{eff} . Both (Friedson & Gonzales, 2017) and (Leconte et al., 2017) explored the impact of condensates forming stable radiative layers. Both carried out linear stability analyses and reached similar findings, concluding that super-critical abundances of H_2O would result in a superadiabatic temperature gradient. Friedson and Gonzales also explored the vulnerability of

these condensation zones to entrainment pressure from the surrounding environment. All of these investigations showed that thermal boundary layers provided a mechanism to trap heat deep within the interior, allowing the envelope above to cool more quickly.

1.1 Condensation in Hydrogen Dominated Atmospheres

Up to now, we have discussed convection as a means of energy transport. We have been using terms 'convection' and 'dry convection' synonymously. From here on, we will be explicit. When we speak of dry convection, we are not taking into consideration the condensation of molecular species in the atmosphere. On Earth, the atmosphere undergoes moist convection. As a parcel of air is lifted, it cools until it gets cold enough that water vapor condenses out, releasing latent heat of condensation which further boosts convection. This release of latent heat alters the temperature-pressure profile of the atmosphere, which now follows a moist adiabat. In addition to altering the temperature gradient, condensation may also create a gradient in mean molecular weight. For example, on Earth, moist air is lighter than dry air. H_2O vapor (molecular mass = 18 g/mol), the primary condensate in Earth's atmosphere, is lighter (not by much) than the background air which is composed primarily of N_2 (molecular mass = 28 g/mol). When H_2O vapor abundance exceeds the saturation vapor pressure, the vapor condenses out of the atmosphere, resulting in a small vertical gradient in mean molecular weight. In Earth's atmosphere, this small gradient does not impose a significant barrier to convection. By contrast, in hydrogen dominated atmospheres such as Neptune and Uranus, the background gas is much lighter than the condensates. In this hydrogen-rich environment, when H_2O condenses out of the atmosphere, a strong vertical gradient in mean molecular weight can be established, resulting

2

Model

2.1 Three-layer Model with Dry Adiabat

We begin our description of the physics of our interior structure model by assuming spherical symmetry and conservation of mass:

$$\frac{dm}{dr} = 4\pi r^2 \rho \quad (2.1)$$

where dm is the mass contained within a sphere of radius $r + dr$, and ρ is the density.

Hydrostatic equilibrium is also assumed and described by:

$$\frac{dP}{dr} = -\frac{Gm\rho}{r^2} \quad (2.2)$$

where P is the pressure and G is the gravitational constant.

We employ a three-layer interior structure, seen schematically in Figure 2.1. At the center of the planet is a core of mass, m_{core} . The core is made of pure water ice, indicated by $Z = 1$, the H₂O mass fraction. Moving outward, the inner envelope is H₂O

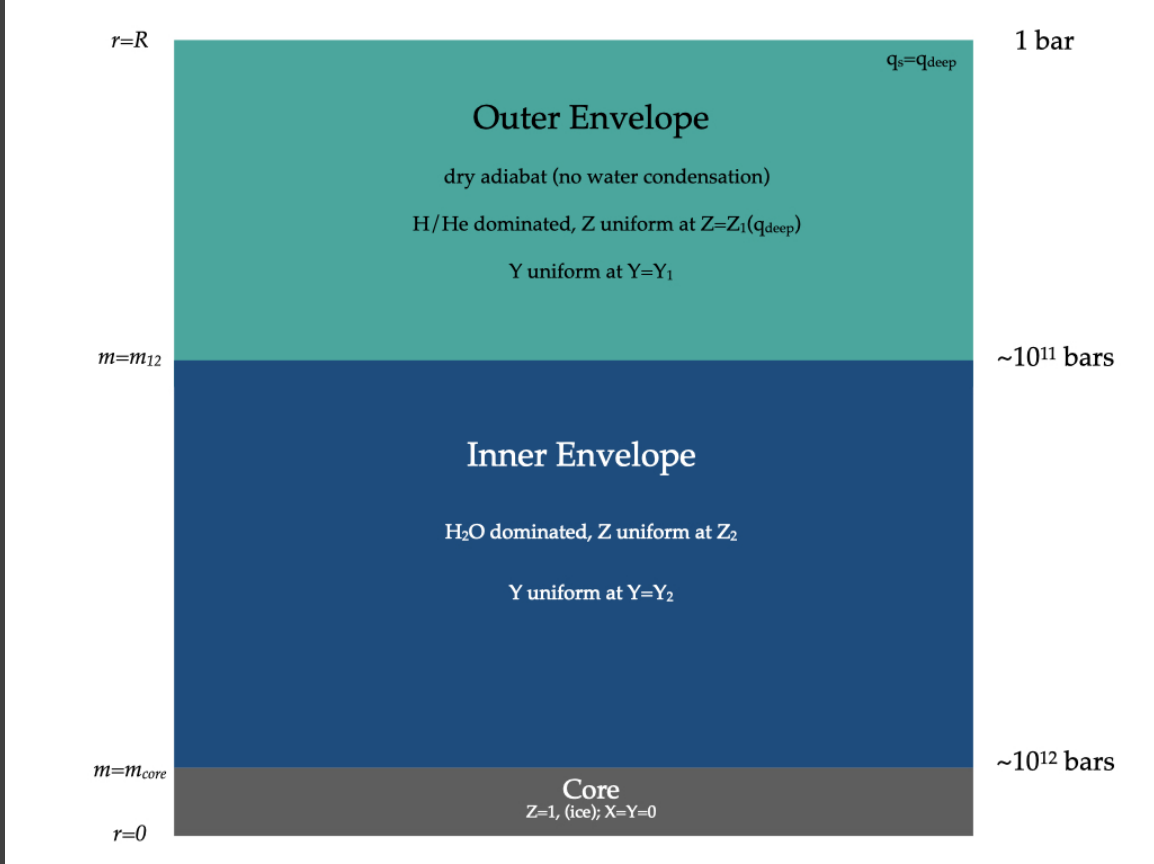


Figure 2.1: A conventional interior structure: Fully convective and dry adiabatic. In this model, the inner and outer envelopes are assumed to be well mixed, fully convective, and following a dry adiabat. The core is composed of water ice. The inner envelope is water dominated, with uniform concentrations of hydrogen, helium, and water; whereas, the outer envelope is hydrogen and helium dominated with trace amounts of water. The atmosphere extends beyond 1 bar, but pressures down to 1 bar are sufficient to capture the formation and impact of the water condensation zones investigated here.

Historically, interior structure models have assumed that the interiors are composed of compressible gases that are fully convective. In a dry-convective model such as this, as a parcel of gas rises, its temperature decreases while its volume increases. This process is known as adiabatic expansion. Conversely, if the parcel sinks, it gets warmer as its

volume decreases. This process is known as adiabatic compression. These processes assume constant entropy. While there may be a critical concentration for a condensable species, this dry model does not allow for condensation. It is said that the temperature-pressure profile follows a dry adiabatic gradient (R. Kippenhahn, 2012), given by:

$$\nabla_{\text{ad}} = \left(\frac{\partial \ln T}{\partial \ln P} \right)_s \quad (2.8)$$

where s is entropy.

Finally, beyond the outer envelope is the atmosphere. Atmospheres regulate how quickly the energy within a planet's interior can radiate into space. When modeling the thermal evolution of gas and ice giants, it has long been recognized that model atmospheres constitute an outer boundary condition for interior structure models, providing key inputs that impact cooling times for interior structure models (Graboske et al., 1975; Fortney et al., 2011). Specifically, model atmospheres allow us to link the planet's T_{int} and T_{eff} to the model's surface gravity, g , and its T_1 or T_{10} . Our work utilizes the (Fortney et al., 2011) model atmosphere.

2.2 Inclusion of Moist Adiabat Within Outer Envelope

Our interior structure model modifies the conventional structure described in Section 2.1 by adding a moist adiabatic layer to the outer envelope, which under favorable conditions, allows for the condensation of H₂O. Gases condense at sufficiently low temperatures or high pressures. Condensation of a gas is characterized by its saturation vapor pressure, which derives from the Clausius-Clapeyron equation (Lavega, 2011). The satura-

tion vapor pressure, P_{sat} , is given by

$$P_{\text{sat}}(T) = P_{\text{sat}}(T_0)e^{-\frac{L+C_p T_0}{R_{\text{vap}}}(\frac{1}{T}-\frac{1}{T_0})-\frac{C_p}{R_{\text{vap}}}\ln \frac{T}{T_0}} \quad (2.9)$$

where $T_0 = 273.16K$, and R_{vap} is the gas constant for the condensable species. When the partial pressure of a gas, P_{gas} , is less than P_{sat} , the parcel of gas is 'subsaturated'. When $P_{\text{gas}} = P_{\text{sat}}$, the gas is 'saturated'. And, when $P_{\text{gas}} > P_{\text{sat}}$, the parcel is 'supersaturated'. Every condensable species has its own saturation vapor pressure. We define the moist adiabat as (Lavega, 2011)

$$\nabla_{\text{moist}} = \left(1 + \frac{\frac{x_{\text{vap}} L}{R_{\text{vap}} T}}{\nabla_{ad} + \frac{L^2}{R_{\text{vap}}^2 T^2}}\right) \quad (2.10)$$

where

$$x_{\text{vap}} = \frac{P_{\text{sat}}}{P} \quad (2.11)$$

and

$$\frac{dT}{dP} = \frac{T}{P} \nabla_{\text{moist}} \quad (2.12)$$

and the gradient of the water vapor mole fraction is given by

$$\frac{dx_{\text{vap}}}{dP} = \frac{x_{\text{vap}} L}{R_{\text{vap}} T^2} \frac{dT}{dP} - \frac{x_{\text{vap}}}{P} \quad (2.13)$$

In Figure 2.3, we compare pressure-temperature and pressure-xvap profiles that follow a dry adiabatic lapse rate, a moist adiabatic lapse rate, and a moist adiabatic lapse rate containing a radiative layer at some depth. The profile of the moist adiabatic lapse rate is cooler at depth than either of the other two profiles. However, the presence of a stable radiative layer results in a warmer interior. These profiles assume $q_{\text{deep}} = 0.25$ and $T_1 = 150K$, which is approximately when the onset of condensation-inhibited convection occurs, as will be shown in Chapter 3. When the pressure-temperature profile follows a dry adiabat, the vapor mole fraction, x_{vap} , is constant.

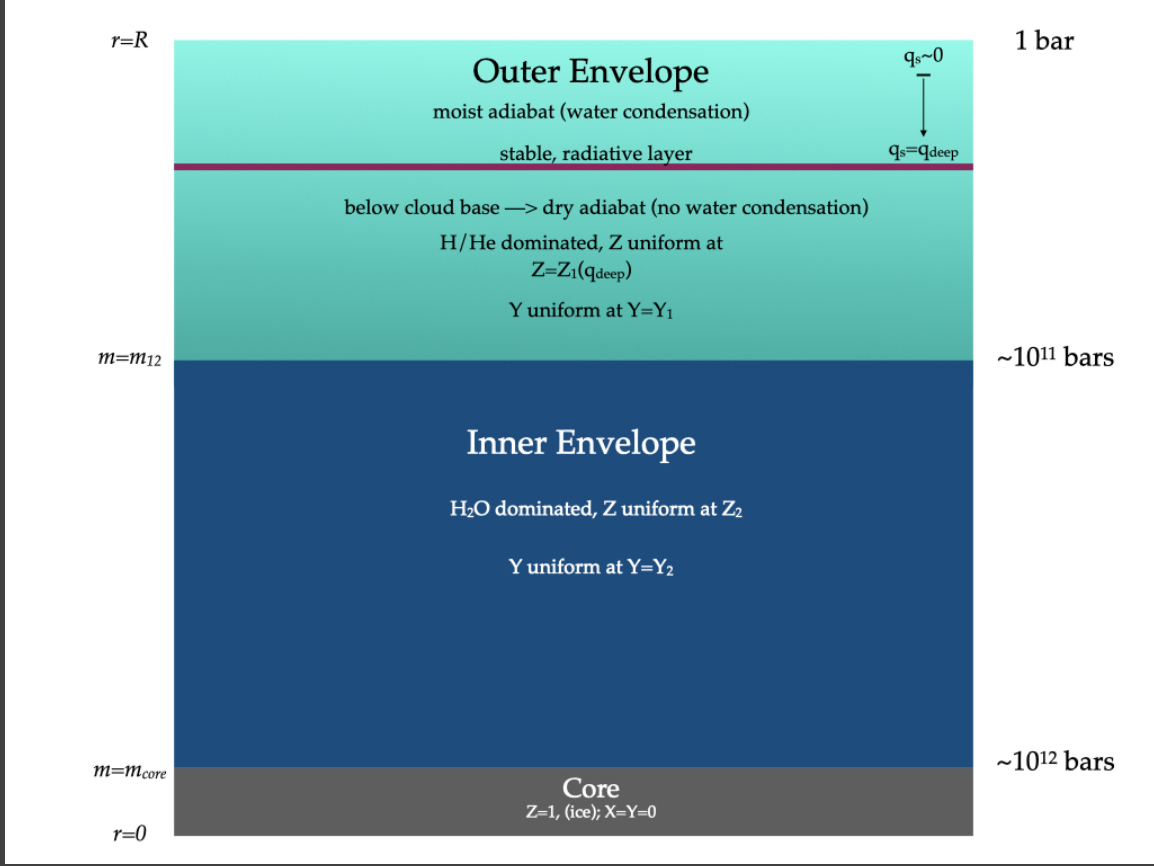


Figure 2.2: The structure for moist adiabatic interior, allowing for condensation-inhibited convection. In this model, a stable water condensation zone may form. The red horizontal line indicates the radiative zone (water condensation zone). The pressure and temperature at the base of the condensation zone is set by the condition that x_{vap} has reached the deep value $x_{\text{vap}}^{\text{deep}}$. Below the condensation zone, the temperature and pressure follow a dry adiabat.

If condensation occurs, our model assumes that it may be stable against convection if a fast rain-out occurs such that the vertical gradient in mean molecular weight is large enough to counteract the positive buoyancy of the parcel of gas (Leconte et al., 2017) (Friedson & Gonzales, 2017). In this scenario, convection is interrupted when α is negative, where α (Friedson & Gonzales, 2017) is given by:

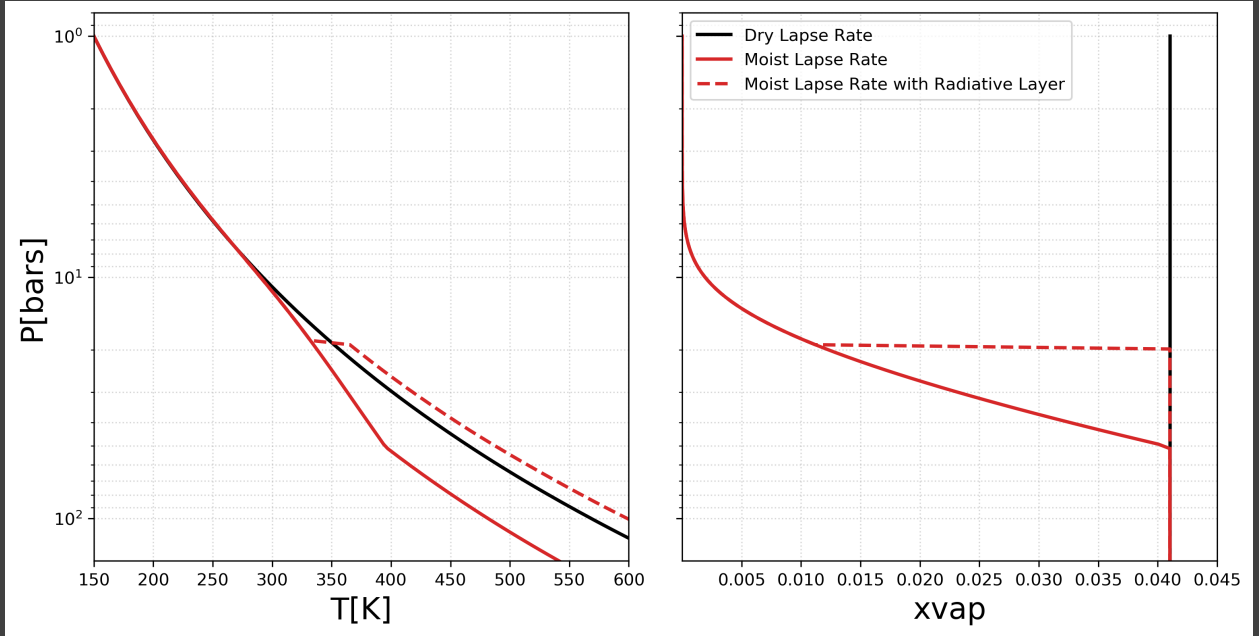


Figure 2.3: The solid red line is the profile following moist adiabatic lapse rate. The solid black line is following the the dry adiabatic lapse rate. The dashed red line is following a moist adiabatic lapse rate with the addition of a stable radiative layer (water condensation zone).

$$\alpha = 1 + \xi(q_s L / R_{\text{vap}} T_0) \quad (2.14)$$

where R_{vap} is the gas constant for the vapor (water), T_0 is the local temperature, L is the latent heat of vaporization for water, q_s is the saturation specific humidity, and ξ is given by $\xi = \frac{1}{\epsilon} - 1$, where ϵ is the ratio of the molecular weight of vapor to the mean molecular weight of dry atmosphere. In our case, $\xi \approx -0.872$. When α is negative, the vertical gradient in molecular weight results in a stabilizing effect, overwhelming the effects due to latent heat release.

2.3 Temperature Jump Across the Water Condensation Zone

In a layer in which alpha, Eqn. 2.14, becomes negative, convection is interrupted. In the limit that H₂O rains out quickly, (Friedson & Gonzales, 2017; Leconte et al., 2017) it has been shown that radiative diffusion is responsible for heat transport, with the temperature gradient across the zone following a radiative temperature gradient (R. Kippenhahn, 2012)

$$\left(\frac{dT}{dP}\right)_{\text{rad}} = \frac{T}{P} \nabla_{\text{rad}} = \frac{T}{P} \times \frac{3}{16} \frac{\kappa_R P}{g} \frac{T_{\text{int}}^4}{T^4} \quad (2.15)$$

Due to the large opacities, κ_R , that are typical of giant planet interiors, the radiative gradient is significantly larger than the either the dry adiabatic gradient or moist adiabatic gradient. This radiative gradient results in a sharp temperature increase as seen with the dashed-red curve in Figure 2.3. Since our model has a finite radial resolution, it is unable to spatially resolve the temperature change. Instead, the model treats the water condensation zone (a thin, stable, radiative layer) as a discontinuous increase in temperature. Nevertheless, this radiative zone corresponds to a continuum of temperatures that is governed by

$$T(P) = T_{\text{top}} + \int_{P_{\text{top}}}^{P_{\text{base}}} \left(\frac{dT}{dP}\right)_{\text{rad}} dP \quad (2.16)$$

with P_{top} and T_{top} denote the pressure and temperature at the top of the stable water condensation zone, and P_{base} represents the bottom of the zone. The radiative temperature gradient across the water condensation zone is nearly constant, so that Eqn. 2.16 simplifies to

$$T_{\text{base}} \equiv T(P + \Delta P) = T_{\text{top}} + \left(\frac{dT}{dP}\right)_{\text{rad}} \Delta P \quad (2.17)$$

where ΔP is the extent of the pressure-space of the water condensation zone (radiative layer), given by

$$\Delta P \equiv P_{\text{base}} - P_{\text{top}} = \frac{P_{\text{sat}}(T_{\text{base}})}{x_{\text{vap}}^{\text{deep}}} - P_{\text{top}}. \quad (2.18)$$

Within the condensation zone, the vapor mole fraction, x_{vap} is equal to the saturated vapor mole fraction:

$$x_{\text{vap}}(P, T) = x_{\text{vap}}^{\text{sat}}(P, T) = \frac{P_{\text{sat}}(T)}{P}, \quad P < P_{\text{base}}. \quad (2.19)$$

The base of the condensation zone is set by the condition that x_{vap} has reached the deep value $x_{\text{vap}}^{\text{deep}}$:

$$x_{\text{vap}}^{\text{sat}}(P_{\text{base}}, T_{\text{base}}) = \frac{P_{\text{sat}}(T_{\text{base}})}{P_{\text{base}}} = x_{\text{vap}}^{\text{deep}}. \quad (2.20)$$

Below the water condensation zone, the region is subsaturated and hence no condensation occurs. Temperatures below the water condensation zone are obtained by integrating the dry adiabat ∇_{ad}

$$T(P > P_{\text{base}}) = T_{\text{base}} + \int_{P_{\text{base}}}^P \left(\frac{dT}{dP} \right)_{\text{ad}} dP. \quad (2.21)$$

2.4 Energy Conservation and Thermal Evolution of Model

Conservation of energy implies that the planet's luminosity, given by

$$L_{\text{int}} = 4\pi R^2 \sigma_{\text{SB}} T_{\text{int}}^4 \quad (2.22)$$

must be balanced by the rate of change of its total internal energy. When we have a sequence of progressively cooler models, we calculate the timestep between any two models using the

3

Results

3.1 Condensation-inhibited Convection

Figure 3.1 shows the results of our initial, exploratory models. We show α with respect to pressure, vapor mole fraction, and temperature. These static models are run for a variety of T_{10} 's, the planet's temperature at $P = 10$ bars. As the bulk water abundance for Uranus and Neptune is unconstrained (Guillot, 1995), the model runs use three different values of q_{deep} , searching for deep water abundances and evolutionary phases for which convection is inhibited by water condensation. In these exploratory models, we only consider the model Uranus. We find that for $q_{\text{deep}} = 0.05$, no condensation-inhibited convection occurs. In other words, α (Eqn. 2.14) never takes on negative values with this concentration of water vapor, hence the condition for stability is never met. However, for larger values of q_{deep} , we find that α does take on negative values (see rows 2 and 3 in Figure 3.1). These finding are in agreement with (Friedson & Gonzales, 2017; Leconte et al., 2017). The shaded regions of the plots indicate the pressure-space over which α is negative. For

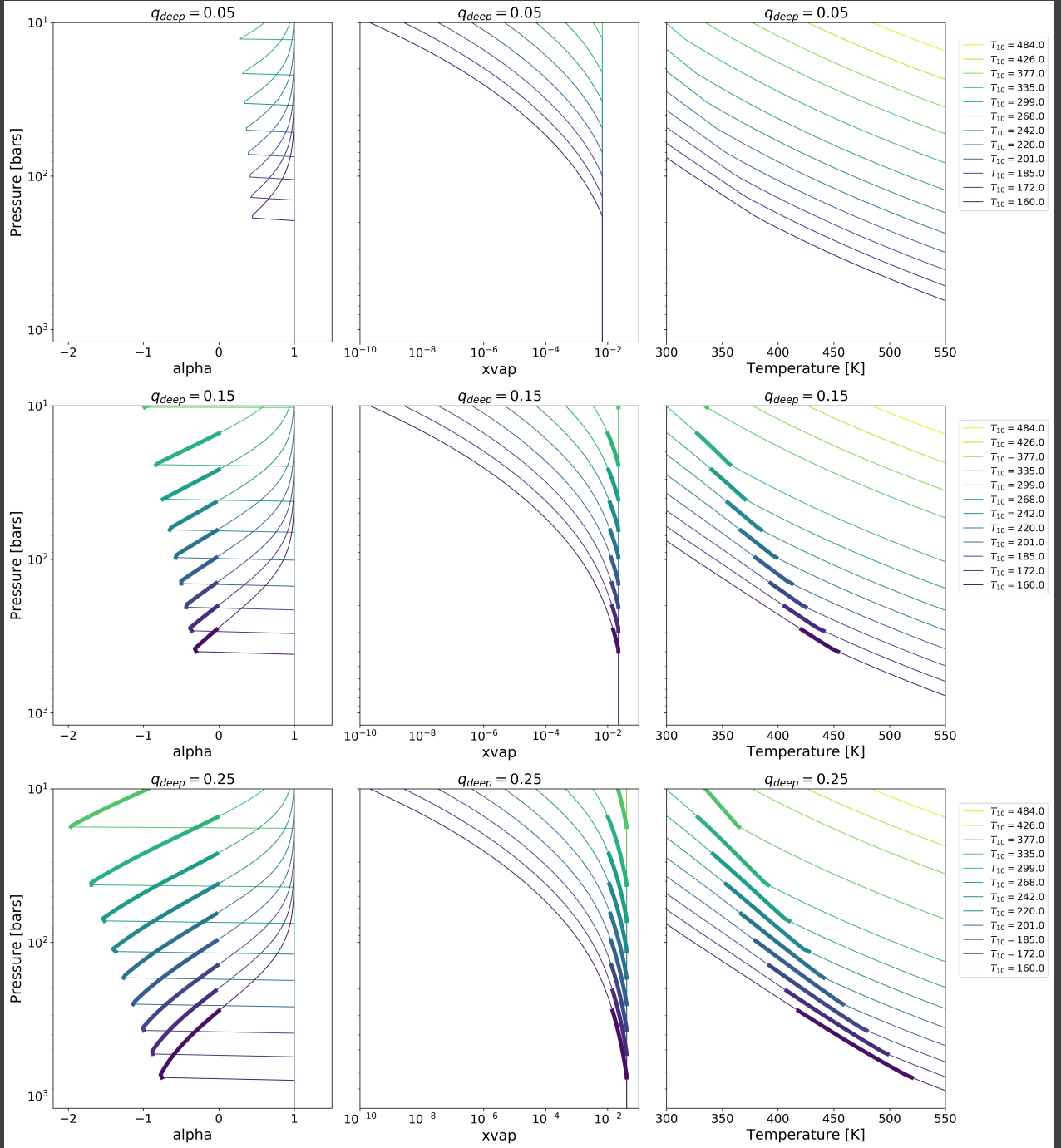


Figure 3.1: Each row represents a different value for q_{deep} . For $q_{deep} = 0.05$, no stable condensation zone forms. For $q_{deep} = 0.15$ and $q_{deep} = 0.25$, convection is inhibited by condensation. The shaded regions show the extent of when α is negative.

which indicates the onset of condensation, at which point the lapse rate has a shallower slope. For the larger values of q_{deep} , where α takes on negative values, we see the onset of condensation-inhibited convection and the establishment of a radiative zone. In the plots, the water condensation zones are represented by the horizontal discontinuities moving from left to right. As the planet cools, these radiative zones descend deeper into the planet's interior. When the radiative zones are established, the interior below the zone becomes much warmer. In Figure 3.2, we highlight the effect of a warming interior. In this figure, we have overlaid the profiles for $q_{\text{deep}} = 0.25$ (exhibiting stable water condensation zones) over the profile for $q_{\text{deep}} = 0.05$ (no stable zones). From this plot, one can see that the presence of a radiative zone creates a temperature jump such that a given T_{10} appears to look like an earlier T_{10} . In other words, we find that the steep temperature increase caused by the presence of a radiative zone causes the interior to be much hotter than one would find using a simple moist adiabatic model with no stable layers. So, for a fixed T_{10} , while sub-critical($q_{\text{deep}}=0.05$) and super-critical ($q_{\text{deep}}=0.25$) models may appear identical near the surface, the super-critical model has a much warmer interior, one that resembles an earlier evolutionary track at a higher T_{10} .

Looking at the adjacent x_{vap} plots, we can see that x_{vap} follows its saturated value. At the bottom of the radiative zone, the vapor mole fraction equals its deep water value, which is the condition that sets the base of the condensation zone.

3.3 Thermal Evolution of Uranus and Neptune

In Figure 3.4, we display the results of evolutionary tracks that consider separately the evolution of a dry adiabat, a moist adiabat with condensation but no stable radiative

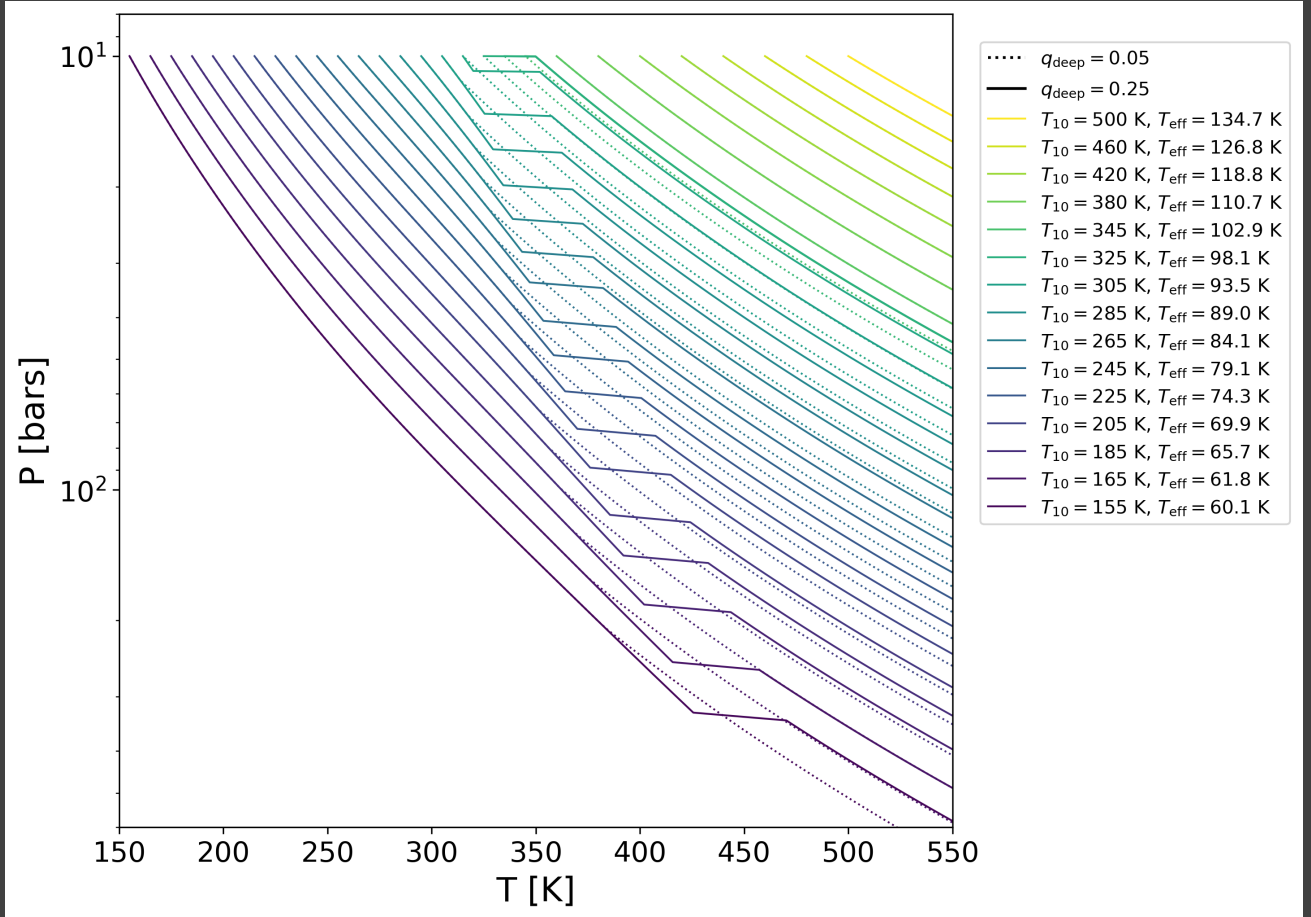


Figure 3.2: The solid lines represent the pressure-temperature profile for $q_{\text{deep}} = 0.25$, and the dashed lines for $q_{\text{deep}} = 0.05$. Looking at recent T_{10} 's, interior temperatures for $q_{\text{deep}} = 0.25$ jump to an earlier T_{10} .

zone, and a moist adiabat with condensation containing stable radiative zones. For all of these evolutionary tracks, we assume $q_{\text{deep}} = 0.25$. Looking at these evolutionary tracks, the coolest scenario at present time, is a moist adiabat that is never stable against convection. The moist adiabat that is stable against convection has the warmest outcome at present time. In Figure 3.5 (Uranus) and Figure 3.6 (Neptune), we consider the impact of different deep water concentrations on the thermal evolution of Uranus and Neptune. As the planets cool, their radiative zones descend deeper into the interior, as we saw in Figure 3.3. This

behavior is also noticeable in the thermal evolution plots. Looking at T_{eff} at 7×10^7 Gyr, the onset of condensation-inhibited convection occurs, resulting in a discontinuous temperature drop. The same behavior is seen in the T_{10} plots for both planets, however, by this time the radiative zone has descended deeper, later in time at around 7×10^8 Gyr. Larger q_{deep} 's result in warmer Uranus and Neptune at present time. We also look at the impact of q_{deep} on the evolution of planetary radius and find that larger values of q_{deep} tend to converge more closely toward the presently observed radius for both Uranus and Neptune in these simulations.

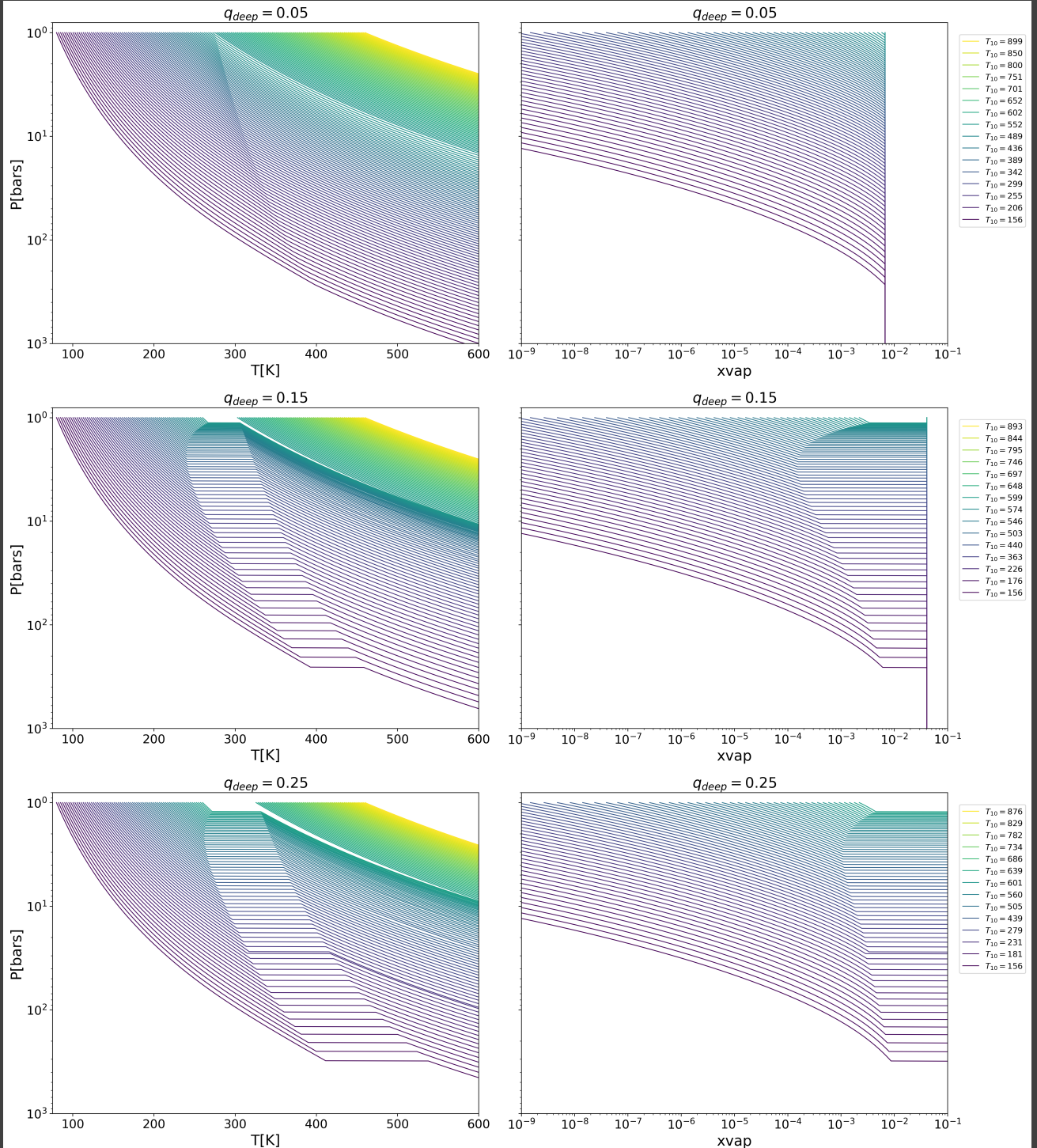


Figure 3.3: These plots were generated using our model Uranus. Again, from top to bottom, we move from $q_{\text{deep}} = 0.05$, 0.15, and 0.25, respectively. T_{10} 's range from hotter (yellow) to cooler (purple), more recent temperatures. For $q_{\text{deep}} = 0.05$, no stable radiative zones are formed. The kink visible in the middle of the top left plot represents the transition from a moist to dry adiabat. Condensation occurs, but no stability is achieved. For $q_{\text{deep}} = 0.15$ and $q_{\text{deep}} = 0.25$, stable radiative zones are formed, as indicated by the discontinuous temperature jumps moving left to right.

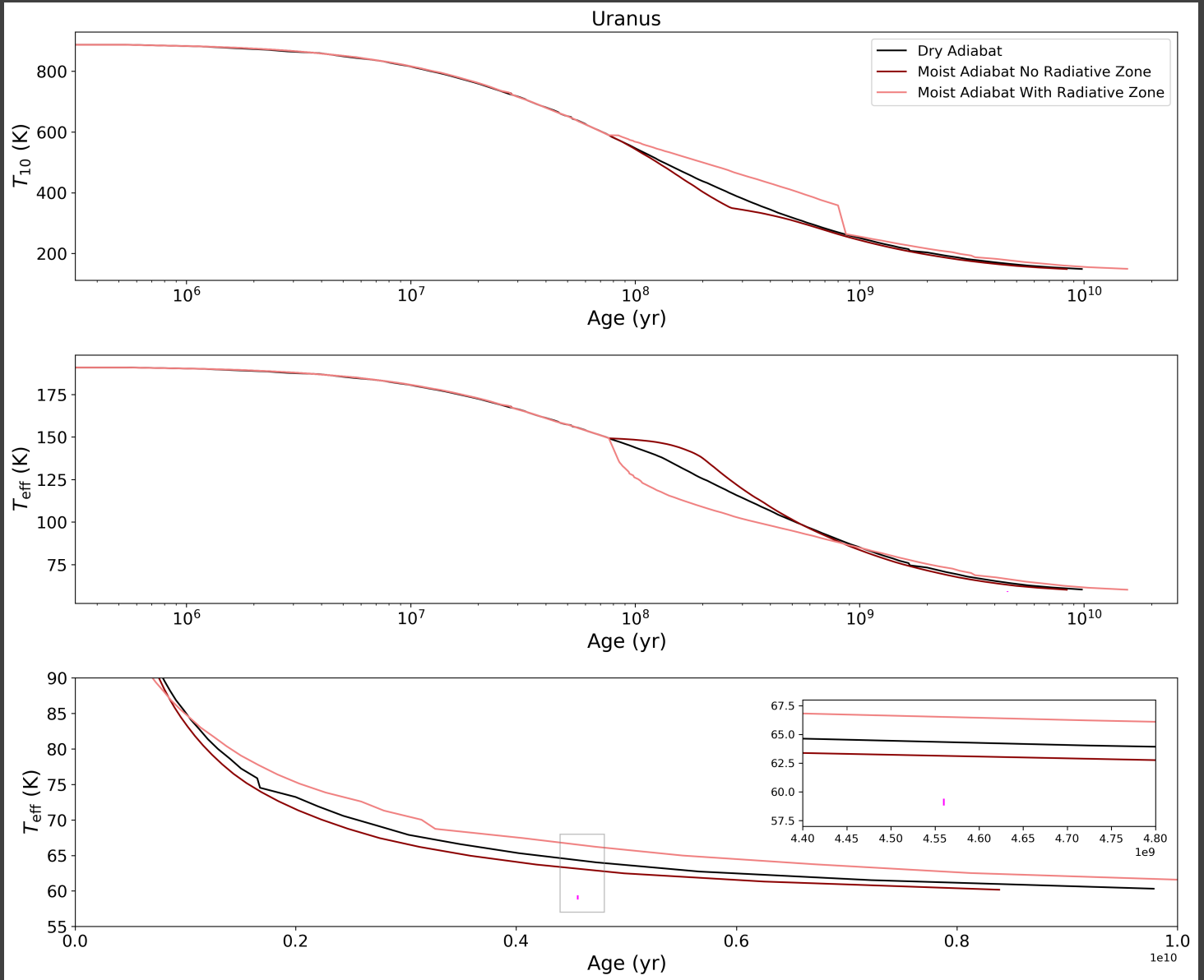


Figure 3.4: The black line represents the thermal evolution for a dry adiabat. The dark red line represents the thermal evolution for a moist adiabat that does not allow for the formation of a stable radiative layer. The light red line represents the thermal evolution of a moist adiabat that does allow for the formation of a stable radiative zone. The fuchsia dot on the lower plot represent the currently observed effective temperature of Uranus with error range.

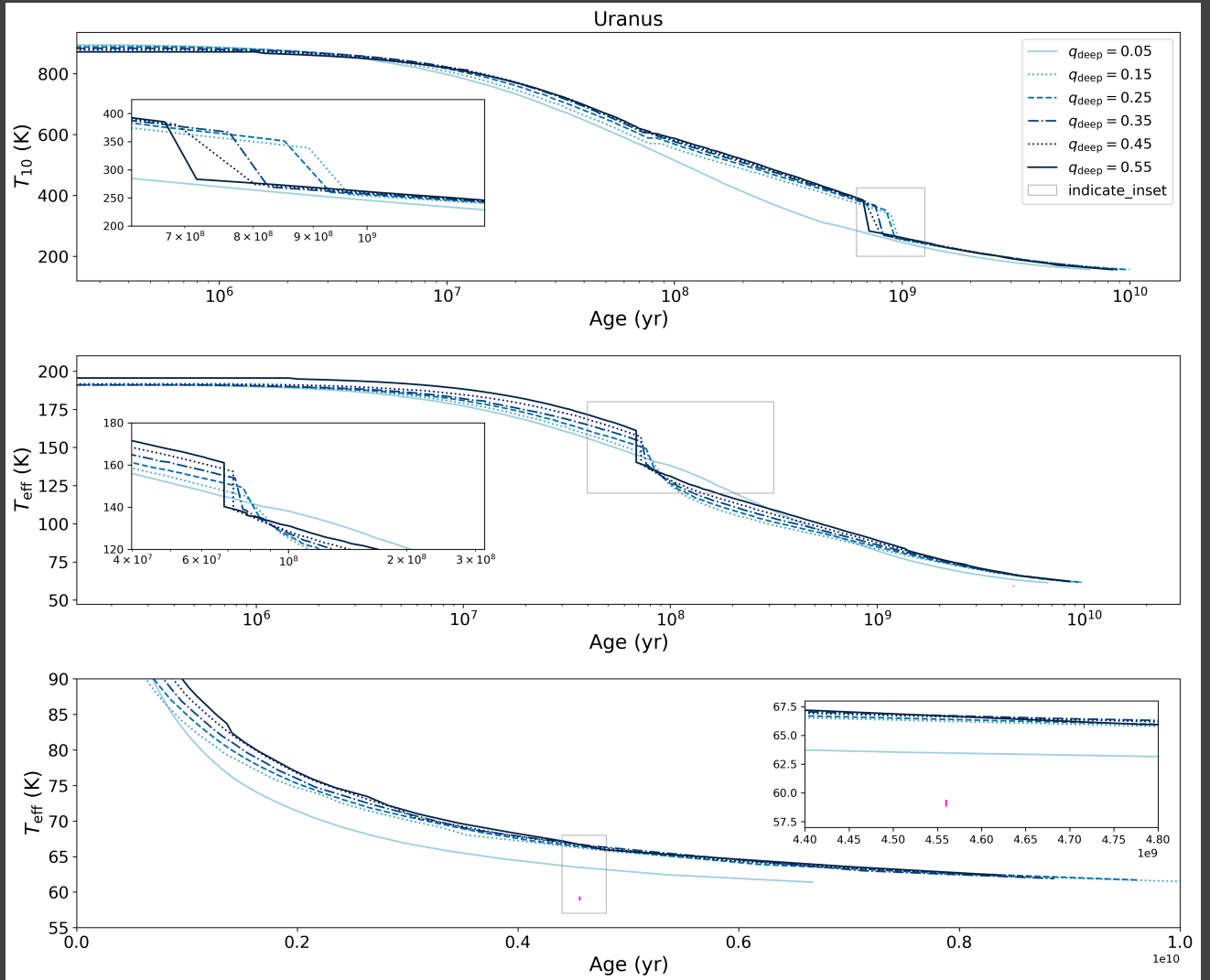


Figure 3.5: The curves in these plots represent thermal evolution tracks for different values of q_{deep} . Dark blue is the largest concentration of water vapor, at $q_{\text{deep}} = 0.55$ and the light blue line is the least concentration of water vapor at $q_{\text{deep}} = 0.05$. For $q_{\text{deep}} = 0.05$, there is no onset of condensation-inhibited convection and no rapid cooling episode. For larger values of q_{deep} there is a rapid cooling episode for T_{eff} at around 7×10^7 Gyr. Similarly, a rapid cooling episode is visible deeper down in the interior as seen in the T_{10} curves at around 8×10^8 Gyr. The insets zoom in on periods of rapid cooling. The vertical fucshia line represents the current T_{eff} with error range.

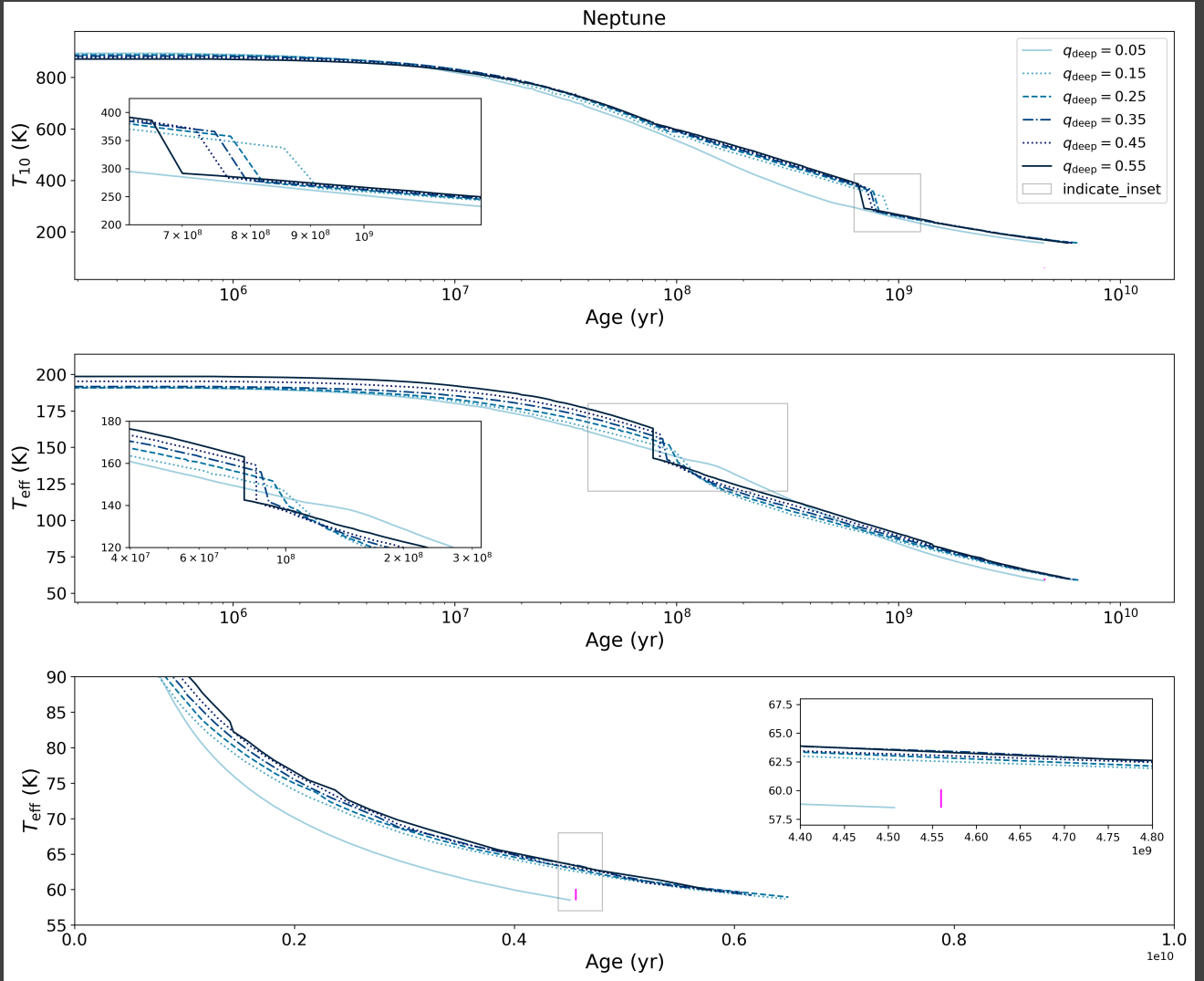


Figure 3.6: Similar to the Uranus plots, The curves in these plots represent thermal evolution tracks for different values of q_{deep} . Dark blue is the largest concentration of water vapor, at $q_{\text{deep}} = 0.55$ and the light blue line is the least concentration of water vapor at $q_{\text{deep}} = 0.05$. For $q_{\text{deep}} = 0.05$, there is no onset of condensation-inhibited convection and no rapid cooling episode. For larger values of q_{deep} there is a rapid cooling episode for T_{eff} at around 7×10^7 Gyr. Similarly, a rapid cooling episode is visible deeper down in the interior as seen in the T_{10} curves at around 8×10^8 Gyr. The insets zoom in on periods of rapid cooling. The vertical fucshia line represents the current T_{eff} with error range.

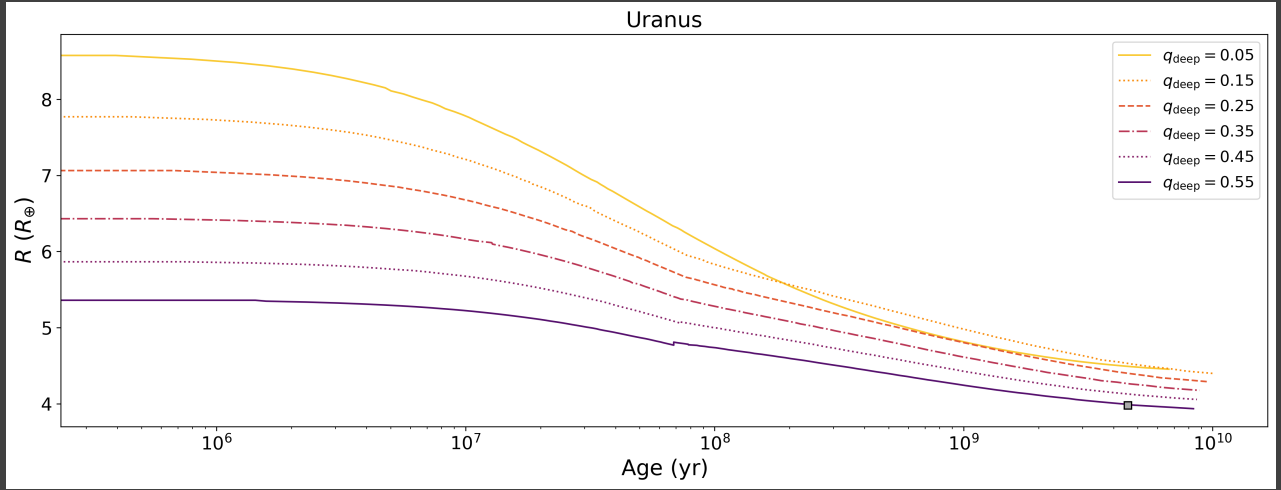


Figure 3.7: This thermal evolution plot shows the impact of different deep water concentration on the radius on model Uranus as it cools. The gray square represents the current observed radius.

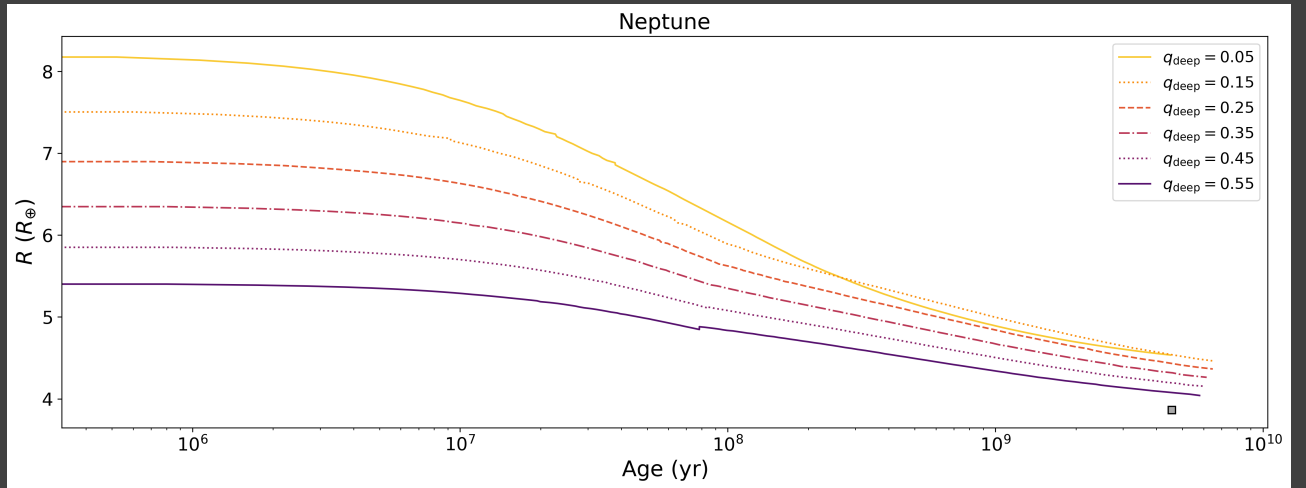


Figure 3.8: This thermal evolution plot shows the impact of different deep water concentration on the radius on model Neptune as it cools. The gray square represents the current observed radius.

4

Discussion and Conclusions

We set out to investigate the impact of water condensation zones on the thermal evolution of our solar system ice giants. It has been speculated that such thermal boundary layers could act as an imperfect insulator, trapping heat below and allowing the envelope above the boundary layer to cool more rapidly (Nettelmann et al., 2016)(Friedson & Gonzales, 2017)(Leconte et al., 2017)(M. Podolak, 1991)(L. Scheibe, 2019). It seems plausible that such interiors could explain the problem with Uranus appearing to have no intrinsic temperature. And, while our analysis suggests that moist-adiabatic inteririors have a significant impact on the heat flow and thermal evolution of ice giants, making a case for the inclusion of moist adiabats in contemporary interior structure models, our findings are nonetheless inconclusive on the problem of Uranus. We do find that incorporating a moist adiabat into our interior structure model does result in a cooler model Uranus and Neptune than would otherwise be seen with a purely dry model. However, when we add stable radiative zones to the interior, we find in the planet's past a period of rapid cooling that results in a cooler effective temperature at around 7×10^7 Gyr. However, both model

Bibliography

- Chabrier, G., Mazevet, S., & Soubiran, F. (2019). A New Equation of State for Dense Hydrogen-Helium Mixtures. *Astrophysical Journal*, 872(1), 51.
- Demarcus, W. C. (1958). The constitution of Jupiter and Saturn. *Astronomical Journal*, 63, 2.
- Fortney, J. J. & Hubbard, W. B. (2003). Phase separation in giant planets: inhomogeneous evolution of Saturn. *Icarus*, 164(1), 228–243.
- Fortney, J. J., Ikoma, M., Nettelmann, N., Guillot, T., & Marley, M. S. (2011). Self-consistent Model Atmospheres and the Cooling of the Solar System’s Giant Planets. *Astrophysical Journal*, 729(1), 32.
- Friedson, A. J. & Gonzales, E. J. (2017). Inhibition of ordinary and diffusive convection in the water condensation zone of the ice giants and implications for their thermal evolution. *Icarus*, 297, 160–178.
- Graboske, H. C., J., Pollack, J. B., Grossman, A. S., & Olness, R. J. (1975). The structure and evolution of Jupiter: the fluid contraction stage. *Astrophysical Journal*, 199, 265–281.

- M. Podolak, W.B. Hubbard, D. S. (1991). Models of uranus' interior and magnetic field. *Uranus, Editors: J.T. Bergstrahl, E.D. Miner, M. Shapely Matthews*, (pp. 29).
- Mankovich, C. & Fortney, J. J. (2019). Evidence for a Dichotomy in the Interior Structures of Jupiter and Saturn from Helium Phase Separation. In *AGU Fall Meeting Abstracts*, volume 2019 (pp. P24B-02).
- Nettelmann, N., Wang, K., Fortney, J. J., Hamel, S., Yellamilli, S., Bethkenhagen, M., & Redmer, R. (2016). Uranus evolution models with simple thermal boundary layers. *Icarus*, 275, 107–116.
- Pearl, J. C. & Conrath, B. J. (1991). The albedo, effective temperature, and energy balance of Neptune, as determined from Voyager data. *Journal of Geophysical Research*, 96, 18921–18930.
- R. Kippenhahn, A. Weigert, A. W. (2012). *Stellar Structure and Evolution*. Springer.
- S. Mazevet, A. Licari, G. C. & Potekhin, A. Y. (2019). Ab initio based equation of state of dense water for planetary and exoplanetary modeling. *Astronomy & Astrophysics*, A128, 621.
- Seager, S. (2010). Exoplanet atmospheres.
- Smoluchowski, R. (1967). Internal Structure and Energy Emission of Jupiter. *Nature*, 215(5102), 691–695.
- W.B. Hubbard, D. S. (1995). The interior of neptune. *Neptune and Triton, Editor: D.P. Kruikshank*, (pp. 109).